THE FLORIDA STATE UNIVERSITY

COLLEGE OF ARTS AND SCIENCES

SOME IMPACTS OF SEAWINDS DATA

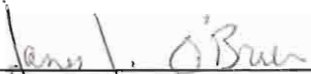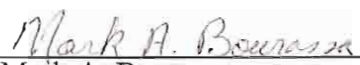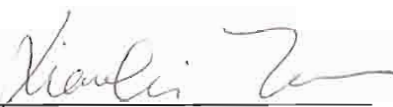IN NUMERICAL WEATHER PREDICTION

By

SHANNON R. DAVIS

A Thesis submitted to the
Department of Meteorology
in partial fulfillment of the
requirements for the degree of
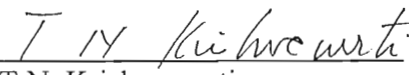Master of Science

Degree Awarded:
Fall Semester, 2002
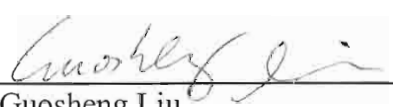
The members of the Committee approve the thesis of Shannon Davis
defended on August 1, 2002

James J. O'Brien
Professor Directing Thesis

Mark A. Bourassa
Committee Member

Xiaolei Zou
Committee Member

T.N. Krishnamurti
Committee Member

Guosheng Liu
Committee Member

This achievement is for my family, Mom, Dad, Xujing, Heidi, Allegro, and Homer and most of all, for my Dad. For the dreams and extraordinary lives we have together, this is just the beginning of much more that I will share with all my heart.

ACKNOWLEDGEMENTS

Acknowledgements don't even begin to touch on the support and love that my family, Mom, Dad Xujing, Heidi, Allegro, and Homer, have shared with me in everything of life. This very true for this work; it has been an experience that we have shared together. Through all times, they have nurtured and inspired me and given me the strength to stay my course and live each moment to the fullest. As Dad says, go for it! Well Dad, I did.

On the work front I want to thank my advisor, James O'Brien, for opening opportunities in the world of ocean and atmospheric sciences and for supporting my studies, my research, and my ambitions during my time at FSU. Mark Bourassa has been the point man in helping me develop this research, and pushing me along the learning curve in a very challenging project.

I wish to thank Xiaolei Zou, T.N. Krishnamurti, and Gousheng Liu for their support on my committee, but most of all, for being outstanding mentors in my coursework at FSU. I also wish to thank the friends and faculty with whom I have shared a special bond with inside the classroom and out. Their support has meant a lot.

TABLE OF CONTENTS

LIST OF TABLES

LIST OF FIGURES

ABSTRACT

Scatterometers can play a significant positive role in the enhancing the performance of Numerical Weather Prediction (NWP) Models. This is shown to be true using scatterometer derived surface pressures as well as the scatterometer surface wind vectors themselves. The separate impacts of sea-surface pressures derived from the scatterometer winds as well as the winds themselves are investigated in an experiment involving one month of assimilated data from NASA's SeaWinds scatterometer. The NASA-NCAR Physics-Space/Finite-Volume GCM is chosen as a suitable medium for this endeavor. The overall performance of the NASA-NCAR GCM suggests that the SeaWinds pressures and winds enhance the model performance in analyses as well as forecasts. The separate impacts of the pressures and winds are nearly equivalent, with the influence of the assimilated winds being slightly stronger.

1. INTRODUCTION

Spaceborne scatterometers provide marine surface wind vector measurements with unprecedented coverage in space and time. As a result, these instruments can serve as invaluable tools in operational meteorology, and yield valuable observations for use in the realm of numerical weather prediction (NWP). Recent work [*Atlas et al.,* 2001] presents a clear review of previous studies which have successfully demonstrated this result. However, these previous works focus solely on the direct assimilation of scatterometer surface winds. Scatterometer winds may also be used to directly calculate sea surface pressure fields [*Endlich et al,* 1981; *Harlan and O'Brien,* 1985; *Brown and Zeng,* 1994; *Zierden et al.,* 2000]. Here, the focus is devoted not only to evaluating the impact the scatterometer winds, but also to the impact of assimilated scatterometer-derived sea surface pressures.

The use of satellite winds for weather prediction has been of great interest since the first spaceborne scatterometer experiments were conducted onboard the space station, Skylab, in 1973 and 1974 [*Moore and Pierson,* 1971]. This interest intensified after the three-month operation of the first unmanned satellite scatterometer, SeaSAT, in 1978. While the longevity of the SeaSAT mission was less than expected, early studies

[*Peteherych et al.,* 1981] remarked about the amazing coverage and detail of marine

1

weather that SeaSAT's surface wind vector measurements revealed. Subsequent launches of European Space Agency (ESA) instruments, ERS-1 in 1991, and ERS-2 in 1995, made scatterometer winds available to forecasters and meteorological centers world wide. These observations greatly aided in making surface analysis and providing advance warnings to weather at sea; however, the effective use of scatterometer winds in NWP models remained a challenge.

Preliminary studies examining the impact of scatterometer data in weather prediction produced only mixed results. *Baker et al.* [1984] and *Duffy et al.* [1984] were amongst the first to establish that assimilated satellite scatterometer winds from SeaSAT-A provided significant improvements in the surface analyses over the oceans. This was particularly true in the case of major synoptic events over the Southern oceans, and other areas where the scarcity of marine observations was most severe. However, the improvements from the SeaSAT winds were less evident in the analysis of upper atmospheric levels, and demonstrated no significant impact on model forecasts. Similar impacts were observed using winds measured by ERS-1. Subsequent works [*Hoffman*, 1993; *Stoffelnson and Anderson*, 1995] demonstrated that ERS-1 surface winds greatly enhanced the initial analysis in the wind fields of the ECMWF model but lacked sufficient influence overall to enhance the model's forecasts. Further studies revealed that the limited impact of scatterometer winds, when assimilated into NWP models, was primarily due to ineffective methods of assimilation. It was realize this was largely related to the unique characteristics of the scatterometer data.

The success of enhancing NWP model performance with scatterometer observations requires the proper consideration of the unique characteristics of scatterometer observations [*Atlas et al.*, 2001]. Satellite surface winds differ from conventional surface wind observations and therefore, require specialized data processing [*Atlas et al.*, 2000]. Satellite scatterometer measurements are indirect observations. They employ an empirically derived geophysical model function to determine wind speed and direction from the signal returned to the radar. Unlike in-situ meteorological observations, scatterometers take measurements in an asynoptic manner. Filtering them into them into synoptic time bins for assimilation or analysis is a poor approximation, particularly at the surface. For these reasons, scatterometer wind data, as with other satellite observations, are difficult to use in sequential assimilation schemes such as optimal interpolation or 3D-VAR in which the horizontal and vertical errors are predefined and do not depend on the meteorological conditions [*Gaffard*, 1996]. More recent studies have proven that scatterometer observations serve most effectively when they have been assimilated in an asynoptic manner [*Atlas et al.*, 1999] or processed using data assimilation schemes such as 4D-VAR that allow for asynoptic observational updates in the assimilation process [*Thepaut et al.*, 1993; *Andrews and Bell*, 1998].

The asynoptic nature of scatterometer measurements has not been the only great obstacle to their effective use in NWP. As surface observations, establishing a means of transmitting their impact into overlying atmospheric layers in the model has been equally challenging. *Atlas et al.* [1996] and *Andrews and Bell* [1998] were amongst the first to pioneer methods to vertically extend the influence of scatterometer surface winds into

pioneer methods to vertically extend the influence of scatterometer surface winds into

upper states in the model. *Atlas et al.* [1996] developed an innovative technique which

3

centered on the empirical derivation of vertical correlation coefficients, by which the mass fields and features in the upper atmospheric layers could be modified in accordance with the scatterometer-influenced surface winds and wind-adjusted surface pressure fields. *Andrews and Bell* [1998] advanced an alternate assimilation scheme, relying on the incremental analysis of the scatterometer winds and corresponding incremental adjustment of state variables such as potential temperature and pressure at each vertical layer for similar purposes. Results from both studies established that the influence of the scatterometer winds could be effectively translated into overlying atmospheric layers. Furthermore, these works clearly demonstrated that the assimilation of scatterometer data in such ways significantly improved the forecasts generated by the model.

This success has continued in more recent works with new innovative methods. In place of vertical correlation or adjustment schemes, sea surface pressures generated from the scatterometers surface winds have been shown to vertically extend the influence of scatterometer observations [*Tahara and Nomura,* 1998; *Tahara,* 2001] in model analyses and forecasts. Preliminary results suggest that the impact of these scatterometer-derived pressures on NWP model performances are even greater than with the use of the winds themselves. Sea surface pressures may be calculated from scatterometer winds using geostrophic relationships and a boundary layer adjustment that are in conjunction with numerical methods of to solve for either pressures or pressure gradients.

Assuming a relatively hydrostatic state in the atmosphere, surface pressures represent three dimensional columns of the atmosphere rather than the two-dimensional fields depicted by the wind vectors alone. Surface pressure fields affect the mass fields of the three dimensional columns of the atmosphere rather than the two-dimensional fields depicted by the wind vectors alone. Surface pressure fields affect the mass fields of the atmosphere directly and thus the impact of their assimilation could be much stronger than

that of the winds alone (without additional model adjustments). With the use of pressures, many issues regarding complicated boundary layer physics can be circumvented and so too the need for any vertical extrapolation schemes to adjust the upper atmospheric levels in NWP models.

Here, the calculation of sea-surface pressures from the scatterometer wind vectors (Section 2.2) is made following the works of *Harlan and O'Brien* [1985], *Brown and Zeng* [1994] and most closely that of *Zierden et al.* [2000]. One month of SeaWinds surface pressures and the same month of winds are assimilated into a global atmospheric model (Section 3) at the National Aeronautics and Space Administration (NASA) Goddard Data Assimilation Office (DAO). It is shown that the impacts of scatterometer-derived pressures and the scatterometer winds themselves vary significantly upon synoptic situations involved. However statistical analysis and case studies strongly suggest that the pressures and the winds have significant and comparable impacts on both the model analyses and model forecast performance (Sections 5 and 6).

2. SEAWINDS INSTRUMENT AND DATA

SeaWinds, like all scatterometers, measures backscattered microwave signals that are
Bragg scattered by short wavelength water waves (capillary and ultra gravity waves) on
the ocean's surface. These short wavelength water waves respond quickly to changes in
wind. The backscattered cross section, σ^o (the fraction of transmitted radar signal energy
reflected back to the instrument), are evaluated with an empirical geophysical model
function that determines surface wind speed and direction relative to the scatterometer's
position. Scatterometers acquire multiple, spatially and temporally co-located
observations of σ^o, from different viewing angles and/or polarizations. This ensures
greater accuracy in measuring wind speed and is necessary for the determination of the
surface wind vector's direction.

With the SeaWinds project, several significant new innovations were incorporated to
enhance the quality and quantity satellite scatterometer measurements. Most notable of
these was the introduction of new radar antenna design. In previous satellite
scatterometers such as SeaSAT, NSCAT, and both ERS instruments, a fan-beam design
employed several antenna's extending away from the spacecraft at fixed angles were
used. However, this design was unable to acquire measurements in the satellite's nadir
employed several antenna's extending away from the spacecraft at fixed angles were
used. However, this design was unable to acquire measurements in the satellite's nadir
region. In contrast to previous instruments, SeaWinds employs a single rotating antenna

6

dish antenna design, which projects two conically rotating pencil beams towards the Earth's surface. These beams have incidence angles of 46.25 and 54 degrees. The resulting inner beam has a radius of 707 km on the surface while the outer beam reaches a corresponding radius of 900 km. Individual "footprints" from SeaWinds are binned into 25X25 km cells, with up to seventy-six cells existing across the width of the instrument's swath. From this geometry measurements are made across a 1800 km swath with greater uncertainty in these measurements occurring in a narrow nadir region as well as the extreme edges of the swath.

2.1 SeaWinds Wind Vectors

Several distinct wind vector data sets are generated from the SeaWinds daily observations. The differences between these data sets lies in the degree of processing applied to original observations, the particular geophysical model function, and input assumptions regarding the satellite position and orientation.

Herein, wind vectors from the SeaWinds Level 2B (L2B) data set are used. These winds are processed at NASA's Jet Propulsion Laboratory (JPL) by the Physical Oceanography Data Acquisition and Archive Center (PODAAC). The model function for obtaining these winds was the QSCAT-1 geophysical model function.

A subset of these vectors (and surface pressures) based on across swath position is assimilated into the model. Previous works [*Atlas et al.*, 1999] identify three primary sub regions of the SeaWinds swath observations, each of these having a different sampling

regions of the SeaWinds swath observations, each of these having a different sampling nature:

- +/- 250 km from the nadir track: poor azimuthal angle diversity for adequate point-wise retrieval,

- 250-700 km from nadir: performance "sweet spot" where number and diversity of the azimuth looks yield best retrieval performance,

- 700-900 km from nadir: vertical polarization only, poor azimuthal angle diversity for adequate point-wise retrieval.

Data (winds or sea-surface pressures) from the 'sweet spot regions" are used exclusively in this experiment. This maximizes the potential impact of the scatterometer data and neutralizes the influence of poorer quality data on the atmospheric model's performance.

2.2 SeaWinds Derived Surface Pressures

The calculation of sea-surface pressures from the scatterometer wind vectors in this study is made following well established variational methods [*Harlan and O'Brien*, 1985; *Zierden et al.*, 2000]. Relative vorticity is computed from scatterometer observations, then it is blended with geostrophic vorticity obtained from a NWP model surface pressure field. New surface pressure fields are found numerically using a method of successive overrelaxation.

The Seawinds wind vector measurements are made on a regular grid aligned with the instrument's surface track, which is convenient for the computation of relative vorticity inside the scatterometer swath. Relative vorticity is computed using a centered finite-

instrument's surface track, which is convenient for the computation of relative vorticity

inside the scatterometer swath. Relative vorticity is computed using a centered finite-

difference scheme. The wind vectors' speed and direction are decomposed into along

track (u') and cross track (v') components. Relative vorticity, ζ_s (scatterometer vorticity), at each interior point in the swath then is:

$$\zeta = (v'_{i+1,j} - v'_{i-1,j})/\Delta x' \quad - \quad (u'_{i,j+1} - u'_{i,j-1})/\Delta y' \qquad (1)$$

where x and y are the cross track and along track locations in the swath, and i denotes the cell position across the swath and j the cell position along the swath . The terms $\Delta x'$ and $\Delta y'$are twice the dimension of the cell size, and remain approximately constant throughout the swath. Delunay triangulation [*Renka,* 1982] is employed to transfer the scatterometer's relative vorticity to a regular quarter degree grid. Grid points where neighboring wind vector data is missing are treated as points without any scatterometer-based relative vorticity.

The scatterometer-based relative vorticity is combined with a geostrophic vorticity obtained from the NWP model before solving for a new sea-surface pressure field. Here, the background geostrophic vorticity is obtained by the relation:

$$\zeta_g = \frac{1}{\rho f}\nabla^2 P + \frac{\beta}{f}u_g \qquad (2)$$

Where P is the NWP surface pressure, ρ is taken as a constant 1.225 kg/m^3 (U.S. Standard atmosphere), f is the Coriolis parameter, $\beta = df/dy$, and u_g is the zonal component of the geostrophic wind. This becomes:

$$\zeta_{gij} = \frac{1}{\rho f_j}(P_{i+1,j} + P_{i-1,j} - 2p_{ij})/\Delta x^2 + \frac{1}{\rho f_j}(P_{i,j+1} + P_{i,j-1} - 2P_{ij})/\Delta y^2$$
$$-\frac{\beta}{f_j^2}(P_{i,j+1} + P_{i,j-1})/2\Delta y \qquad (3)$$

in centered finite difference form. The determination of NWP geostrophic vorticity is

in centered finite difference form. The determination of NWP geostrophic vorticity is

made on the same grid that the NWP pressure. All subsequent steps in the method are

calculated on a finer 0.25 degree grid to maximize the benefit from the scatterometer resolution.

Once both relative scatterometer and NWP geostrophic vorticities are obtained, they are blended together smoothly through the minimization of the cost function (F) to find solutions P_{ij} and ζ_{ij},

$$F(P_{ij}, \zeta_{ij}, \lambda_{ij}) = \sum_i \sum_j \lambda_{ij} \left(\left(\frac{1}{\rho f} \nabla^2 p + \frac{\beta}{f} u_g \right) - \zeta_{ij} \right)$$
$$+ \sum_i \sum_j \frac{K_\zeta}{2} (V_{ij})^2 + \sum_i \sum_j \frac{K_E}{2} G(P_{ij}), \tag{4}$$

where all terms on the right hand side of the equation are summed over the entire domain.

The leading term $\zeta_g = \frac{1}{\rho f} \nabla^2 P + \frac{\beta}{f} u_g$ on the right hand side of the equation is a strong constraint representing the model, multiplied by a Lagrange multiplier [*Sasaki*, 1970]. The second term, minimizes the data misfits (V_{ij}) between the new vorticity (ζ_{ij}) of the solution pressure field and the data (NWP model background or SeaWinds data).

$$V_{ij} = \zeta_{ij} - \frac{1}{R} \zeta_{Sij}, \text{ (in the swaths)} \tag{5}$$

$$V_{ij} = \zeta_{ij} - \zeta_{gij}, \quad \text{(outside the swaths)} \tag{6}$$

The term R is a reduction factor used to adjust relative vorticity at the surface to a geostrophic equivalent [*Zierden et al*, 2000].

The final term on the right hand side of equation (3) is a regularization term, serving to horizontally smooth the solution pressure field. Without this term, the only solution is λ=0, and satellite vorticity is inserted directly into the field. In general, the regularization

λ=0, and satellite vorticity is inserted directly into the field. In general, the regularization term involves the second derivative of the solution field, often in the form of a Laplacian smoother. In this case, however, the Laplacian of P is included in the model and another

penalty function must be used. In this case, kinematic geostrophic kinetic energy, $G(P_{ij})$, is minimized [*Harlan and O'Brien*, 1985].

$$G(p_{ij}) = \frac{1}{2}(u_g^2 + v_g^2) = \frac{1}{2\rho^2 f^2} \nabla P \bullet \nabla P \qquad (7)$$

The coefficients K_ζ and K_E in (4) are weights that control the balance between the amount of smoothing to be done and the data misfits. Letting $K = K_E/K_\zeta$ leads to:

$$\frac{1}{\rho f_j}(P_{i+1,j} + P_{i-1,j} - 2P_{ij})/\Delta x^2 + \frac{1}{\rho f_j}(P_{i,j+1} + P_{i,j-1} - 2P_{ij})/\Delta y^2$$
$$-\frac{\beta}{f_j^2}(P_{i,j+1} + P_{i,j-1})/2\Delta y - \frac{K}{2\rho f}(P_{ij} - P_{0ij}) = \zeta_{Sij} \quad , \qquad \text{(in the swath)} \qquad (8)$$

and

$$\frac{1}{\rho f_j}(P_{i+1,j} + P_{i-1,j} - 2P_{ij})/\Delta x^2 + \frac{1}{\rho f_j}(P_{i,j+1} + P_{i,j-1} - 2P_{ij})/\Delta y^2$$
$$-\frac{\beta}{f_j^2}(P_{i,j+1} + P_{i,j-1})/2\Delta y - \frac{K}{2\rho f}(P_{ij} - P_{0ij}) = \zeta_{gij} \quad . \qquad \text{(outside the swath)} \qquad (9)$$

which are solved using successive overelaxation and constant normal derivative boundary conditions.

3. MODEL

The NASA DAO and the Global Dynamics Division (GDD) of the National Center for Atmospheric Research (NCAR) have recently developed a global circulation model, the NASA-NCAR GCM, which is highly suitable to explore the impact of scatterometer data on NWP. This model was developed in hopes of producing a unified climate, numerical weather prediction, and chemistry transport model suitable for the global data assimilation and simulation of the physical and chemical state of the Earth's atmosphere. Its suitability for the experiments conducted here lies in its robust CORE data assimilation system (DAS) and its Physical-space Statistical Analysis System (PSAS). These systems are designed with the assimilation of satellite observations in mind.

The NASA-NCAR GCM employs a Lagrangian vertical coordinate system, with 55 vertical layers and a horizontal grid with $1.0° \times 1.0°$ resolution. The general circulation model and the Core DAS of the NASA-NCAR model are both based on the finite volume dynamical core [*Lin and Rood*, 1996; *Lin*, 1997; *Lin and Rood*, 1998]. Further physical parameterizations were added to this foundation from the NCAR Community Climate Model 3 (CCM3) [*Kiehl et al*, 1996]. The NASA-NCAR GCM also makes use of a Statistical Quality Control (SQC) System to screen observational data prior to

Model 3 (CCM3) [*Kiehl et al*, 1996]. The NASA-NCAR GCM also makes use of a

Statistical Quality Control (SQC) System to screen observational data prior to assimilation. Essentially, the SQC system is comprised of simple checks of the

observational against a background field. This is followed by an adaptive buddy check which adjusts the error bounds according to the flow of the day.

The analysis system for the NASA-NCAR GCM is an updated version of from the Phyiscal-space Statistical Analysis System (PSAS). In previous studies, the PSAS has proven to be highly successful in enhancing model performance using scatterometer wind observations [*Atlas et al.*, 1999, 2000, 2001], functioning in conjunction with NASA's older GEOS model systems which preceded the NASA-NCAR GCM.

The PSAS combines a first guess from the model with observational data to provide an updated state of the atmosphere. The system works in both observation and finite-volume spaces, with no intermediate constant pressure transformation necessary (P to σ interpolations are eliminated). The PSAS produces analysis increments directly on the model grid, thereby preserving the balance relationships implied by the error covariance formulations. Furthermore, the surface and the upper-air analyzes are unified in the system; thereby, ensuring the consistency between surface pressure and low-level geopotential height analysis, and maximizing the impact of surface wind observations on the upper-air fields.

For the experiments described here, the model assumed its standard configurations with some slight modifications. In place of the full vertical resolution of 55 layers, the model was run with 36 vertical layers, and its horizontal resolution was similarly reduced slightly to $1.0° \times 1.25°$ grid spacing. This configuration is chosen to economize computational time and space.

computational time and space.

4. SEAWINDS IMPACT EXPERIMENTS

A series of individual experiments are conducted to separately assess and compare the impact of assimilated SeaWinds-derived sea surface pressures and assimilated SeaWinds surface wind vectors. The method closely follows the procedures established by [*Atlas et al., 2001*]. The experiments occurred in three separate stages. The first stage is comprised a control run (CR) of the model conducted without any assimilated scatterometer data; thereby establishing a baseline of comparison for ensuing trials. The second stage is the model run with assimilated SeaWinds wind vectors (WR). Correspondingly, the third stage consists of the model simulation with assimilated SeaWinds surface pressures (PR).

An approximately one month period of study (November, 2000) is selected from to examine the scatterometer data's impact on the model performance. During this period, 29 days of scatterometer data are separately assimilated into the model. Assimilations occurred at regular six-hour intervals. From these assimilations, 174 individual global analyses are made as well as 22 individual five-day forecasts. These 22 forecasts were made daily from November 4th to November 25th.

5. RESULTS

The impact of the scatterometer data upon the NASA-NCAR's GCM's performance is evaluated in two phases. Initially, the influence of the SeaWinds data upon the model's analysis fields is investigated (Section 5.1). The impacts the assimilated pressures and winds upon the model's forecasts are subsequently explored (Section 5.2).

5.1 SeaWinds Impact on the GCM's Analyses

Averaged differences between the PR, WR, and the CR analyses are computed globally for the period of the experiment, providing an initial indication of the impact of the SeaWinds assimilations. These globally averaged mean differences (GAMDs) are determined at six hour intervals for parameters at the surface, 850 hPa, and 500 hPa levels. From the GAMDs, mean values, standard deviations in the differences, 90th percentile values, and 10th percentile values are then obtained (Table 1.) Results from these computations reveal the largest differences between the CR and the PR and WR occur in the lower atmospheric layers of the model. Ninetieth percentile values of SLP and 850 hPa geopotenital heights reach 4 +/-0.2 hPa and 24 +/- 3 m respectively. At 500

----- in ---

and 850 hPa geopotenital heights reach 4 +/-0.2 hPa and 24 +/- 3 m respectively. At 500 hPa, the magnitudes of the 90th percentile geopotenital height GAMDs are roughly 60%

less. Similar differences are seen in the analyses of the u and v wind components as well as potential temperature. This is consistent with the expectation that there exists a vertical gradient in the impact of the SeaWinds data on the model analyses. That is, the impact of the scatterometer data on the model analyses progressively weakens with increasing distance from the surface layer.

GAMDs between the two SeaWinds model runs (i.e. PR-WR) are less than those between the SeaWinds runs and the CR (Table 2). Still, while the scales of the GAMDs are small, these differences do reflect globally averaged values. As such, these small variations infer that there is a significant impact produced through the assimilation of the SeaWinds pressures and winds. Values of the GAMDs suggest that this impact may be sufficiently large to question the scatterometer data's suitability for use in the model for climate applications.

Examination of the model analyses on the smaller synoptic scale reveals substantial impacts of the assimilated SeaWinds data. The use of the assimilated SeaWinds data significantly enhances the definition (i.e., relative fine scale features) of developing systems in the analysis fields. Many key features, such as the low pressure centers of developing storms or the frontal locations associated with such storms, can only be seen in the analyses with the assimilated SeaWinds pressures and winds.

A representative example is seen in the eastern Pacific, in the last week of the experiment. Beginning at 12Z on November 22nd, the SeaWinds analyses show a strong low pressure system is observed at 69° S latitude with a central pressure of roughly 967 hPa centered about 155° W longitude (Fig. 5). Associated with this large system are two

hPa centered about 155° W longitude (Fig. 5). Associated with this large system are two

smaller lows, emerging off the southeastern coasts of Australia and New Zealand

16

respectively. In the 12Z CR analysis, these smaller associated systems appear to be nearly identical to in location, size and developmental state to the PR and the WR systems. As the systems evolve, differences (PR-CR and WR-CR) increase. PR and WR SLP analysis fields at 18Z show clearly defined pressure centers for each of these smaller systems; however, these deeper centers are absent in the CR analyses. At 0Z and 6Z (November 23rd), PR and WR analyses show these systems intensifying, whereas the CR analyses suggest a weaker development. This remains true until the 18Z analysis of November 23rd. Validation of these enhancements is made thorough comparison with SSMI observations. However, a shortcoming of the scatterometer-aided analyses for this case is that a similar impact is not observed at either the 850 hPa or 500 hPa pressure levels for this case. This result is typical for the majority of cases and is without any bias towards latitude.

An examination of point to point differences as a function of SLP demonstrates the conditions under which the SeaWinds data impacts on the analyses are greatest. Impacts of the assimilated pressures are largest in regions of strong low surface pressures (Fig. 6). PR analyses of SLP show differences as large as 8 hPa from the CR values for surface lows ranging from 950 to 960 hPa. Substantially larger impacts are seen in a similar analysis made with respect to the Wind Run. Individual differences (WR-CR) in analyzed SLP reach as much as 14hPa. Still, this impact varies in geopotential height and potential temperature fields at 850 and 500 hPa levels for both SeaWinds aided analyses. Furthermore, the differences between the separate PR and WR analyses are largest over the same, extreme low pressure range (Fig. 8). In analyzed SLP, these differences can be

the same, extreme low pressure range (Fig. 8). In analyzed SLP, these differences can be

as much as 9 hPa. These PR-WR differences, as well as the impacts of the SeaWinds data

on the analysis fields, follow the same vertical gradient that is apparent in the GAMD evaluation.

The largest impacts of assimilating either form of scatterometer data are related to the development of major storms, particularly those developing at sea. We see that the changes introduced by the assimilated SeaWinds surface pressures are not as large as those introduced by the SeaWinds surface winds in the analyses produced by the model. The difference in the impacts appears to vary with the intensity the pressure gradients. During the development of stronger low pressure systems, the analyses produced using the assimilated winds typically feature more deeper, more finer centers and gradients (i.e., fronts). The analyses generated using the assimilated pressures smooth the definition of these features, and damp the magnitude of low pressure centers and pressure gradients. This smoothing is likely to be related to the variational method employed in deriving the SeaWinds based pressures. Corrections to this method to improve this smoothing effect and adjust the scatterometer pressures to ageostrophic situations have been advanced [*Patoux et al.,* 2002] and can be applied to reduce this problem in subsequent studies.

5.2 Impact of the Assimilated SeaWinds Data on the Model Forecasts

In addition to the 29 days of 6-hour analyses generated during the experiment, 22 five day forecasts are also made for each model series (PR, WR and CR). Forecasts are generated after the 18Z analysis of each day, commencing on November 5th and ending on November 25, 2000. The observable impacts vary significantly from the global to generated after the 18Z analysis of each day, commencing on November 5th and ending

on November 25, 2000. The observable impacts vary significantly from the global to synoptic scale, and they also exhibits dependence on the synoptic situations involved.

An initial evaluation of the forecasts results is made by computing anomaly correlations (ACS) over the five day forecast period. Specifically, ACSs are computed for the forecasted SLP and 500 hPa geopotential height fields. Particularly when used over short tome periods (less than a week), the ACS evaluates the agreement between forecasted fields and analyzed fields at the same time, thus providing a measure of the internal consistency observed in the forecast process. Verification for the ACS computation is provided by the same model run's analysis (i.e., verification of the PR forecasts is made with the PR analysis fields). These calculations are made separately for the Northern and Southern Hemispheres. Higher ACS values typically infer a better overall model performance, or at least a more consistent one. It is generally accepted that ACS values of 0.60 and higher demonstrate consistent (useful) forecast skill when applied in this manner.

The average ACS computations suggest that that the impact of the scatterometer pressures and winds on the forecasts is very slight in the Northern Hemisphere. It is clearly more pronounced in the Southern Hemisphere (Fig. 9). The average ACS values indicate that the WR forecasts are typically an improvement over the CR in both hemispheres. However, the PR ACSs only show a very slight improvement in the Northern Hemisphere. In the Southern Hemisphere, the assimilated PR forecasts show relatively low ACS values in comparison to the other model runs. However, since different analyses were used in each ACS determination, the lower ACS values do not indicate a poorer forecast accuracy.

indicate a poorer forecast accuracy.

Examination of four separate forecasts shows that the performance varies substantially day by day (Fig. 10a). Forecasts generated from the November 9th analysis indicate that the use of the assimilated pressures improves skill of the forecast by 12 hours in both the Northern and Southern Hemispheres. The WR forecasts made on the same day show slight improvement over the CR in the Northern Hemisphere but have only mixed results in the Southern Hemisphere. Forecast based on the November 12th analysis show a slightly different situation: the assimilated SeaWinds data has substantial impact in the near as well as far ranges of the forecast. The PR ACS of the SLP for the Northern Hemisphere shows a marked improvement in the forecast skill for more than two days towards at the end of the forecasted period. While the wind-aided forecasts show negligible enhancement in the Northern Hemisphere, the ACS analysis for this same forecast cycle shows enormous improvement using the winds in the Southern Hemisphere. Further variation which is seen in the forecasts made on the 18th and 22nd of November (Figs. 10c, d). This variability is typical of all the forecast cycles made, clearly indicating large case to case variability in performance.

Statistical inspection of the fields forecasted in the model illuminates further physical differences the PR and WR forecasts. Forecasted surface parameters of SLP and surface temperature reveal relatively 90th percentile GAMDs of 5 +/- .25 hPa and 1.5 +/-.05 K respectively. Standard deviations of the mean differences are two orders of magnitude lower than the mean values of the differences themselves At the 500 hPa and 850 hPa levels, forecasted geopotential height and potential temperature fields exhibit similar characteristics. Forecasted total precipitation and vertical velocity (omega) also

similar characteristics. Forecasted total precipitation and vertical velocity (omega) also follow this pattern with an order of magnitude increase in the uncertainty. A steady

increase in the standard deviation for these differences further suggests that the two fields (PR and WR) diverge as the forecast period progresses.

Slightly more insight into the variability of the PR and WR forecasts is evident in examination of their differences as a function of SLP. As observed in the model analyses, noticeable differences between the PR and WR SLP fields occur in the forecasts for strong low pressure systems (Fig. 13). Similar differences are found on 850 hPa and 500 hPa geopotential heights. In other fields, such as total precipitation and vertical velocity, a different pattern is seen. While clear tendencies are seen in the height and SLP fields, offsetting differences are apparent in precipitation and vertical velocity differences. There is a steady diminishing of the mean differences moving from the 850 hPa to the 500 hPa level; similar to what is observed in the model analysis fields. Thus, the differences in the impacts become less pronounced with height for most model fields.

The forecasts made on November 22nd provide a representative example of the forecast results. Two days into the forecast of the 22[nd,] a strong low pressure system develops off the southeast coast of Greenland and due West of the British Isles (Fig. 14). At the 6Z on the 24th, the forecasted SLP and geopotential heights are nearly identical in both the PR and WR forecasts. In the more sensitive fields of vertical velocity and precipitation, this similarity is evident as well. This similarity is maintained as the system develops over 12 hours, moving in a westward direction.

The ACS analysis suggests there is a large difference between the separate impacts of the assimilated SeaWinds pressures and winds; however, case studies indicate that this difference is less than expected in regions where the SeaWinds data plays its most

difference is less than expected in regions where the SeaWinds data plays its most significant role. In examination of individual events occurring during the experimental

period, only small differences were apparent between the forecasted fields produced by the pressures and those produced by the winds. The greatest difference between wind and pressure run occurs in strong systems; however, these differences are small compared to the systems' perturbations from the mean. These results indicate that the NWP model has greater internal consistency with the scatterometer derived winds. Inspections of differences in several parameters at the 850 hPa and 500 hPa levels suggest that these differences become less evident farther above the surface layer.

6. CONCLUSIONS

This study of the impacts of SeaWinds data on the NASA-NCAR GCM indicates that satellite scatterometers can play a significant and positive role in the realm of NWP. This is true in the case of utilizing either SeaWinds derived pressures or SeaWinds surface wind vectors. The impacts of the pressures on analyses and forecasts are similar, but not identical to that of the winds.

In the analysis phase of the model performance, the impact of both pressures and winds is observed in globally averaged statistics calculated for many different model fields. The magnitude of these many differences are small (on the order of 0.5%), and the standard deviation of these GAMDs is relatively constant. That is, the impact yielded from the use of the SeaWinds data was steady throughout the course of the experiment. However, one of the applications of the model is climate application, which would likely be sensitive to such changes.

A more detailed analysis of the differences between the SeaWinds analyses and the Control, shows that the largest impacts of the scatterometer data are observed in the analyses of strong low pressure systems. In deep lows (i.e., 940 hPa), differences in analyzed SLP as large as 14 hPa exist between the scatterometer-aided analyses and the analyzed SLP as large as 14 hPa exist between the scatterometer-aided analyses and the CR. Similarly, these strong low pressure events also present the conditions under which

the analyses using the pressures and the analyses using the winds differ the most. Differences in SLP at the same 940 hPa interval are as much as 8 hPa between the PR and the WR. Differences between the scatterometer analyses and the CR as well as between the PR and WR analyses themselves are evident in geopotential height and potential temperature fields at upper levels as well. There is a distinct vertical gradient in these differences, reaffirming the expectation that the scatterometer data's impact diminishes in the analyses of upper atmospheric layers, but is far away from negligible at 500 hPa. The differences in the separate impacts of the pressures and winds on the analyses are similarly less in these upper atmospheric layers as well.

On synoptic scales, the initial impact of the scatterometer pressures and winds is manifested as an improved analysis of developing marine storms, fronts and strong low-pressure systems. In terms of anomaly correlation scores (ACSs), more of an impact is yielded from the assimilated winds than from the assimilated pressures, indicating a greater internal consistency with assimilation of the wind product. Both show noticeable improvement over the CR analyses. However, in examination of identical features in PR and WR analysis fields, it is seen that the PR analysis exhibits smoothing of some synoptic scale systems and some damping of their intensity. This may be related to the smoothing applied in the method used to derive the SeaWinds pressure fields, which could be alleviated with very recently developed techniques that better account for ageostrophic terms. These differences are less apparent in the model forecast fields.

ACS analysis suggests that on average, the SeaWinds data positively enhanced the model forecasts, particularly in the Southern Hemisphere. The greatest average ACS model forecasts, particularly in the Southern Hemisphere. The greatest average ACS values are seen in WR forecasts. However, it is evident that the performance of both the

pressures and winds varies substantially on a case by case basis. As is seen in the analyses, the separate impacts of the pressures and winds on forecasts appear greatest in cases of strong low pressure systems. The differences in gridded forecast fields are typically smaller than differences between analysis fields. Much of the smoothing apparent in the PR analyses is less evident in the forecasts.

The results of this study are expected to be highly dependent upon the atmospheric model used and the data assimilation method employed to incorporate the scatterometer data. Future studies using different models and different data assimilation techniques would strongly enhance the findings explored here. This experiment demonstrates the benefits of the DAO's data assimilation system, particularly with regard to scatterometer data. The assimilation of scatterometer pressures is a unique aspect of this study and results suggest that the assimilation of the pressures is nearly as effective as the assimilation of the winds in this setup. The impact of the pressures is expected to be greater in less sophisticated NWP assimilation and analyses systems.

1a) **Globally Averaged Differences Statistics (PR-CR)**

Field	Mean	Standard Deviation	90th percentile value	10th percentile value
Sea Level Pressure (hPa)	2.23	0.18	3.37	-3.72
Surface Temperature (K)	0.93	0.05	1.78	-3.24
Geopotential Heights at 850 hPa (m)	18.13	3.18	22.05	-33.25
Geopotential Heights at 500 hPa (m)	9.37	0.67	20.37	-34.39
Potential Temperature at 850 hPa (K)	1.25	0.41	1.85	-2.45
Potential Temperature at 500 hPa (K)	0.91	0.33	1.44	-2.20
U Wind Component at 850 hPa (m/s)	1.43	0.24	2.01	-2.37
U Wind Component at 500 hPa (m/s)	0.33	0.09	0.93	-0.95
V Wind at 850 hPa (m/s)	0.29	0.10	0.81	-0.91
V Wind at 500 hPa (m/s)	0.18	0.09	0.25	-0.10

1b) **Globally Averaged Differences Statistics (WR-CR)**

Field	Mean	Standard Deviation	90th percentile value	10th percentile value
Sea Level Pressure (hPa)	3.04	0.24	3.95	-3.41
Surface Temperature (K)	0.95	0.05	1.88	-3.30
Geopotential Heights at 850 hPa (m)	22.25	3.25	24.09	-37.9
Geopotential Heights at 500 hPa (m)	9.75	0.71	9.33	-12.39
Potential Temperature at 850 hPa (K)	1.28	0.43	2.25	-3.05
Potential Temperature at 500 hPa (K)	0.44	0.09	1.24	-2.83
U Wind at 850 hPa (m/s)	1.49	0.25	2.22	-2.73
U Wind at 500 hPa (m/s)	0.33	0.09	0.93	-0.95
V Wind at 850 hPa (m/s)	0.33	0.10	0.83	-0.93
V Wind at 500 hPa (m/s)	0.22	0.09	0.37	-0.25

Table 1. Statistics derived from Globally averaged mean differences (GAMDs) in the model analyses fields. 1a) Statistics derived from PR-CR differences 1b) Statistics

Table 1. Statistics derived from Globally averaged mean differences (GAMDs) in the model analyses fields. 1a) Statistics derived from PR-CR differences 1b) Statistics derived from WR-CR differences

26

PR-WR statistics derived from Globally averaged differences

Field	Mean	Standard Deviation	90th percentile value	10th percentile value
Sea Level Pressure (hPa)	1.83	0.20	3.43	-3.37
Surface Temperature (K)	0.71	0.05	1.38	-3.30
Geopotential Heights at 850 hPa (m)	9.25	2.24	22.09	-33.41
Geopotential Heights at 500 hPa (m)	5.33	0.67	18.43	-28.77
Potential Temperature at 850 hPa (K)	0.78	0.41	1.85	-1.83
Potential Temperature at 500 hPa (K)	0.83	0.24	1.37	-2.51
U Wind Component at 850 hPa (m/s)	0.98	0.09	1.88	-1.38
U Wind Component at 500 hPa (m/s)	0.24	0.08	0.25	-0.43
V Wind Component at 850 hPa (m/s)	0.33	0.06	.95	-1.33
V Wind Component at 500 hPa (m/s)	0.18	0.07	0.22	-0.37

Table 2. PR-WR statistics derived from Globally averaged mean differences (GAMDs) in the model analyses fields.

Differences (SeaWinds-CR) in analyzed SLP as a function of PR SLP
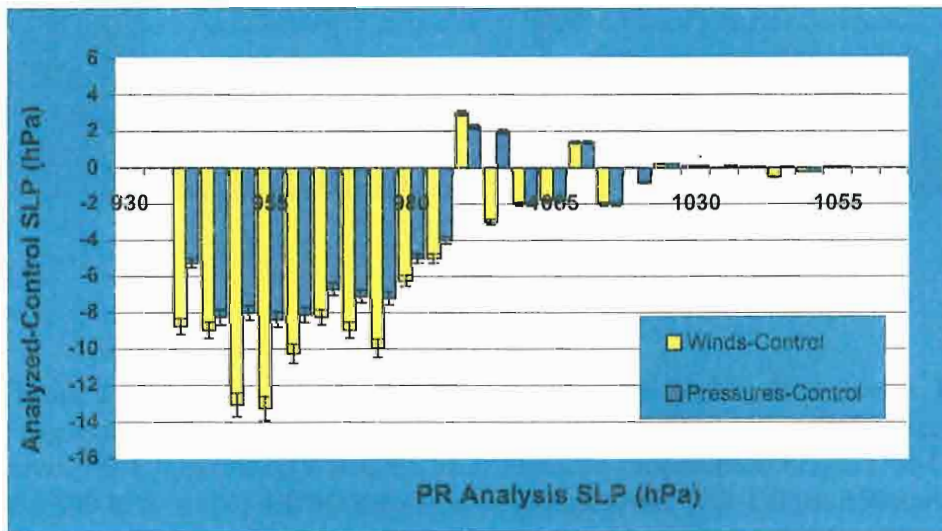
Figure 1. Evaluation of the impacts of assimilated SeaWinds pressures and winds on the model analyses at the surface as a function of PR SLP values: (blue:(PR-CR);yellow:(WR-CR); Error bars denote +/- one standard deviation.
and winds on the model analyses at the surface as a function of PR SLP values: (blue:(PR-CR);yellow:(WR-CR); Error bars denote +/- one standard deviation.
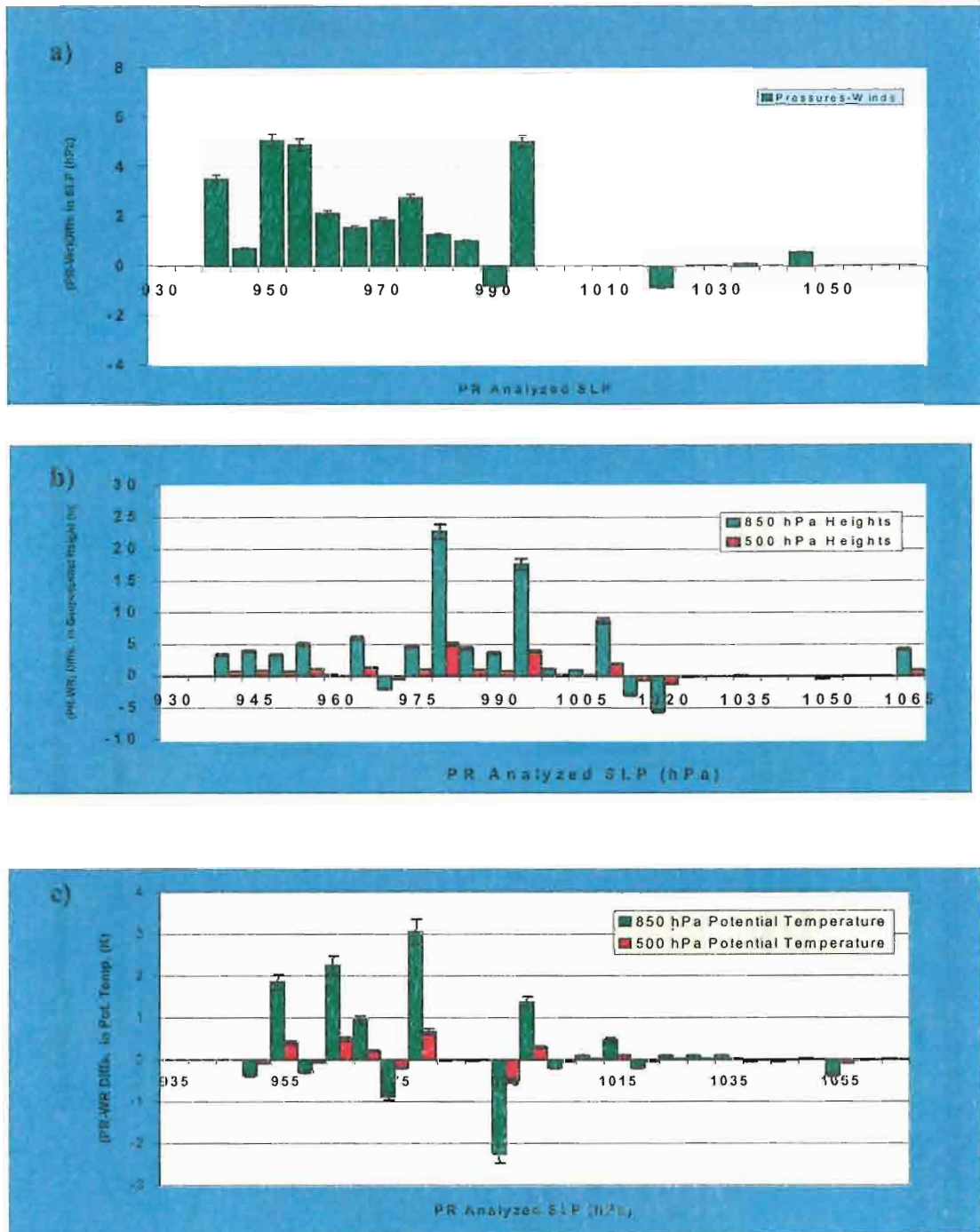
Differences (PR-CR) above the surface as a function of PR SLP
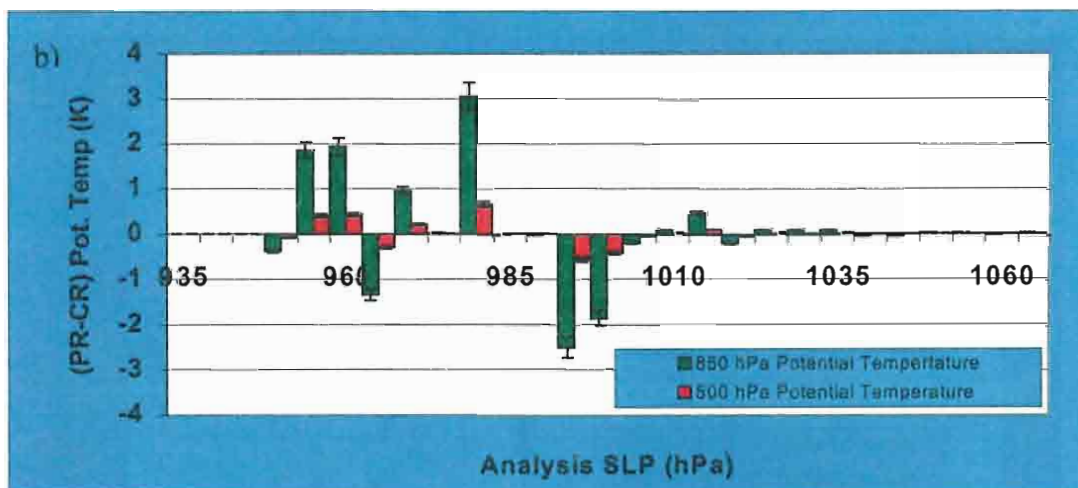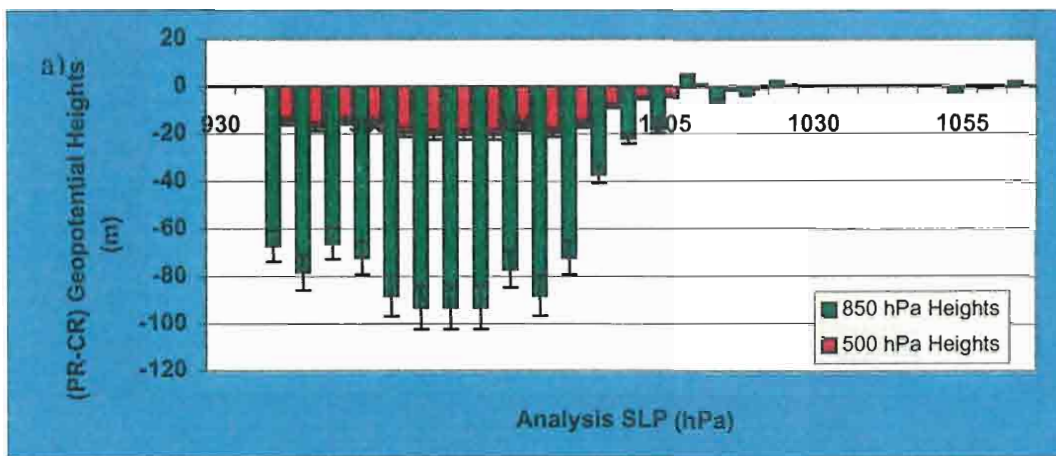
Figure 2 : Evaluation of the impacts of assimilated SeaWinds pressures, PR-CR, as a function of PR SLP values: a) differences in surface pressure difference (blue:(PR-CR);yellow:(WR-CR); b) differences geopotential height (PR-CR) at 850 and 500 hPa; and c) differences potential temperature (PR-CR) at 850 and 500 hPa. Error bars denote +/- one standard deviation.
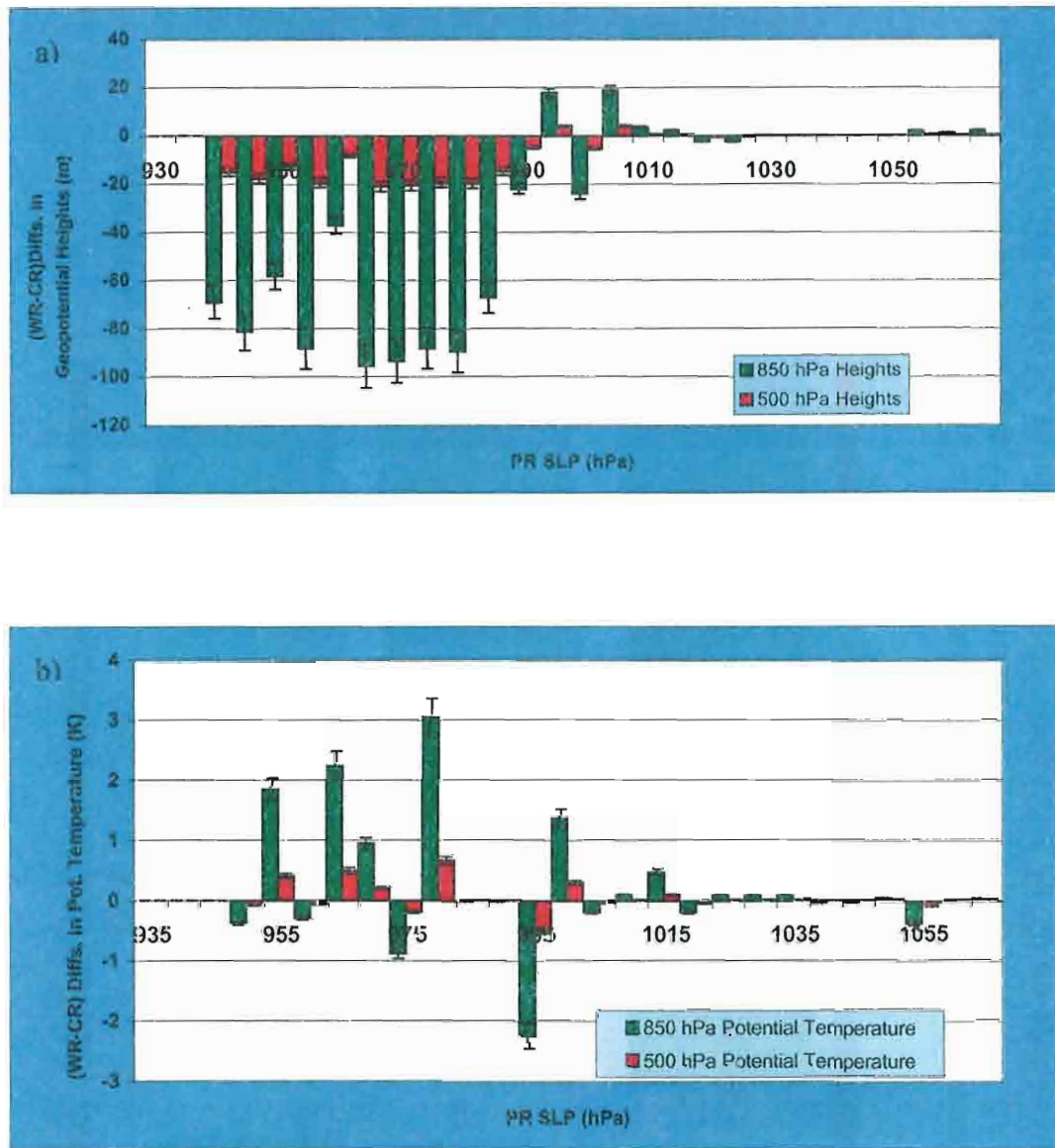
Figure 3 : Evaluation of the impacts of assimilated SeaWinds winds, WR-CR, as a function of PR SLP values: a) differences geopotential height (WPR-CR) at 850 and 500 hPa; and b) differences potential temperature (PR-CR) at 850 and 500 hPa. Error bars denote +/- one standard deviation.

Error bars denote +/- one standard deviation.

Case Study of the SeaWinds Data's impact on the Model Analyses
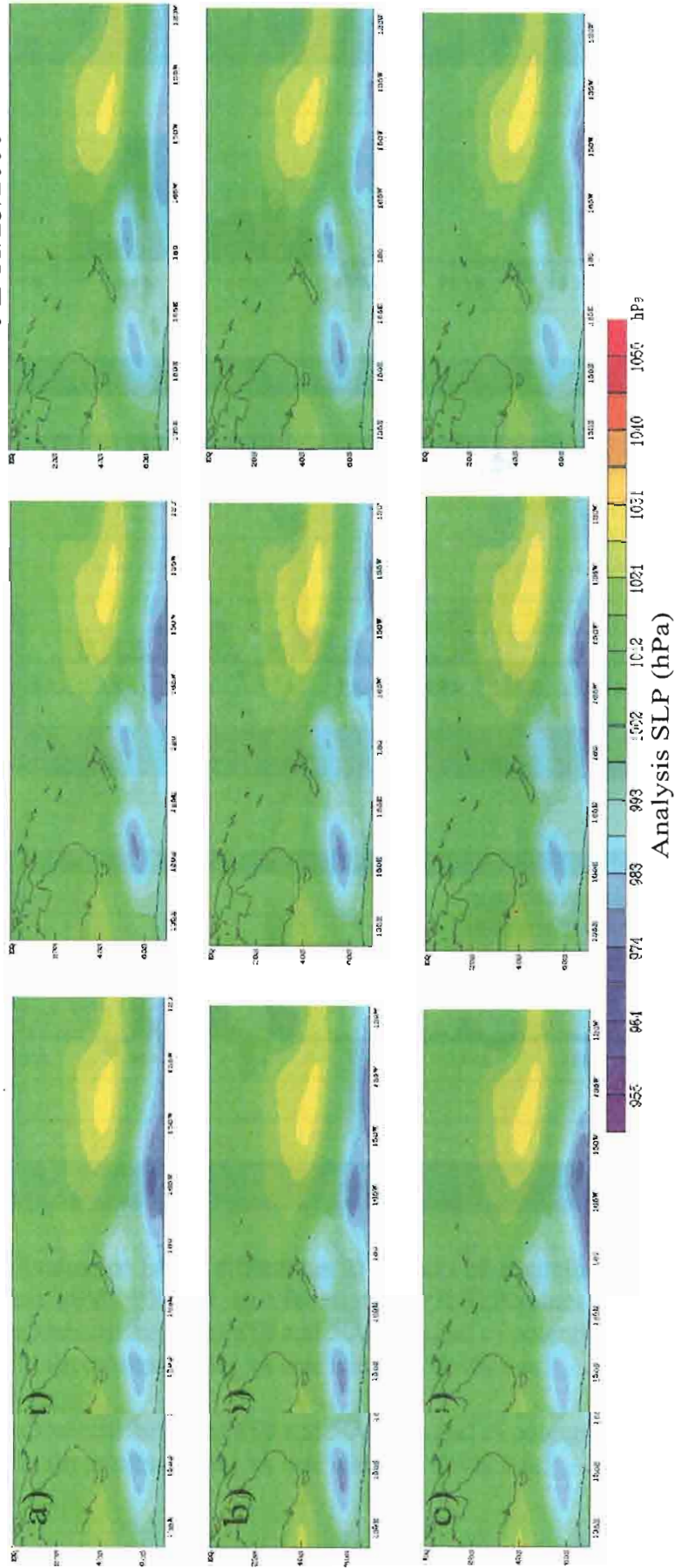
Figure 4. Case study in the Eastern Pacific exemplifying the impact of the SeaWinds pressures and winds on the NASA/NCAR GCM's surface analyses. Three snap shots taken 6 hours apart beginning on 12Z of 11/22 and ending on 0Z of 11/23 show the SLP analyses of a) the PR, b) the WR, and c) and c) the CR. Note the well defined pressure centers evident in both the PR and WR and not in the CR.

Mean Differences (PR-WR) as a function of PR SLP

Figure 5 : Evaluation of the differences in impacts of assimilated SeaWinds pressures and winds, PR-WR, as a function of PR SLP values: a) differences in SLP; b) geopotential height at 850 and 500 hPa; and c) potential temperature at 850 and 500 hPa. Error bars denote +/- one standard deviation.

SLP; b) geopotential height at 850 and 500 hPa; and c) potential temperature at 850 and 500 hPa. Error bars denote +/- one standard deviation.

Anomaly Correlations (ACSs) of SLP and 500 hPa Geopotential Heights

Computed for the Average of 21 Forecasts
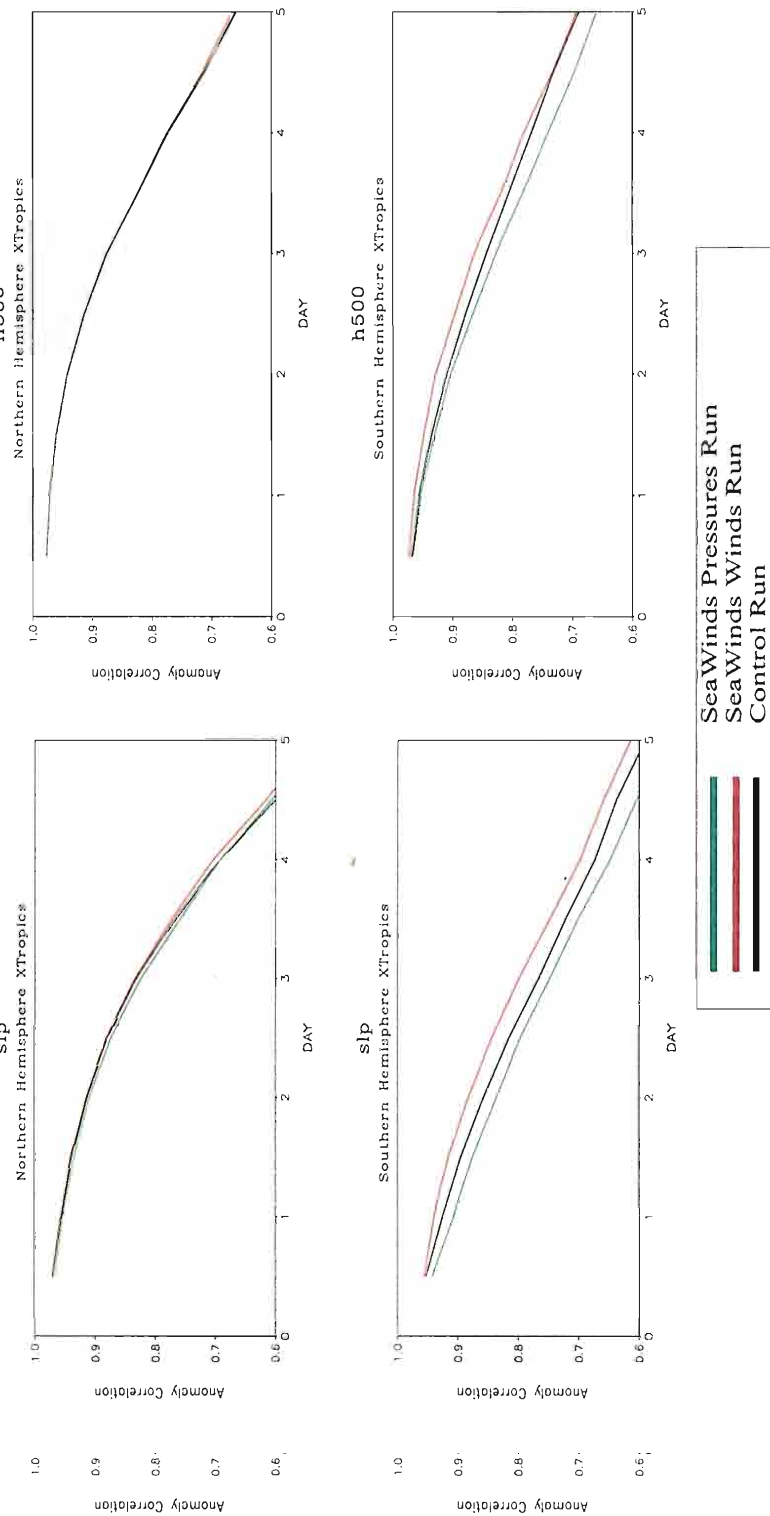
Figure 6: Anomaly corellations of SLP and 500 hPa geopotential heights determined for the average of 21 forecasts made for each of the three model runs (Control Run, Pressures Run, Winds Run)
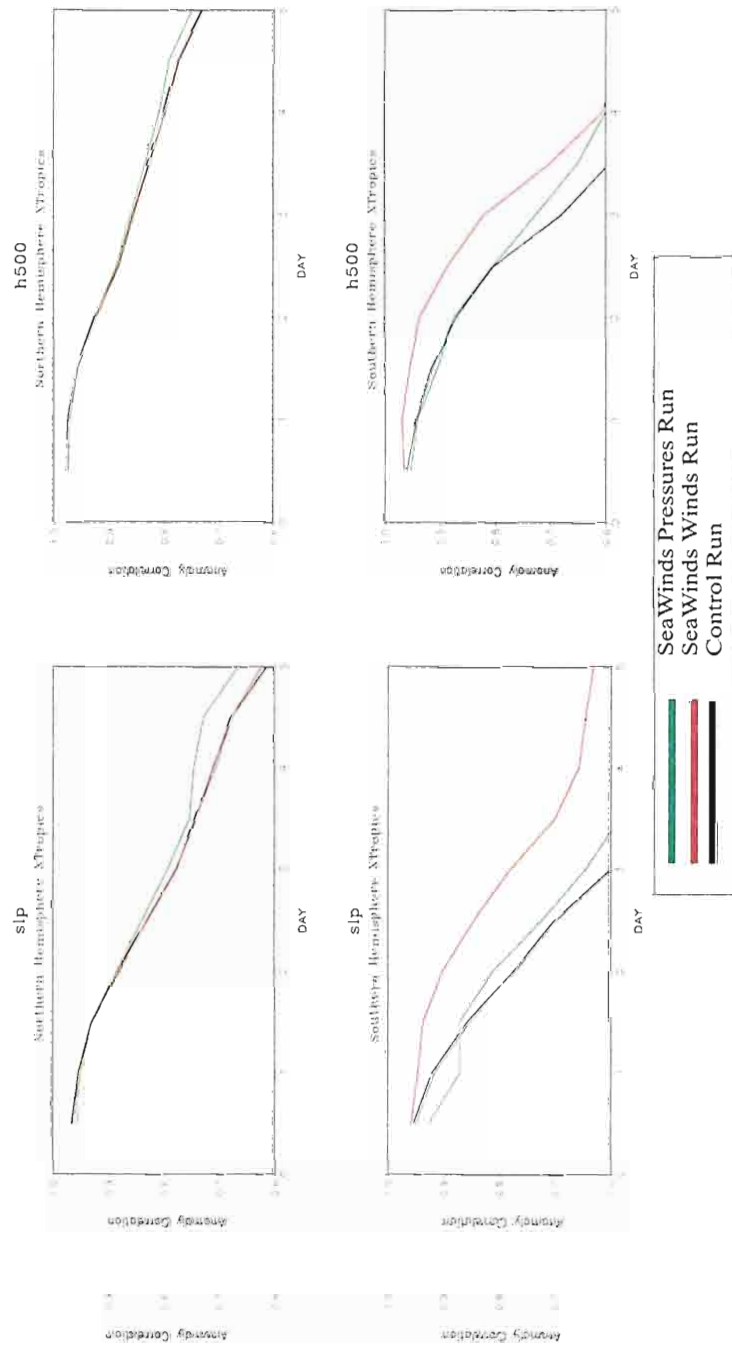
Representative ACSs computed for four individual forecasts
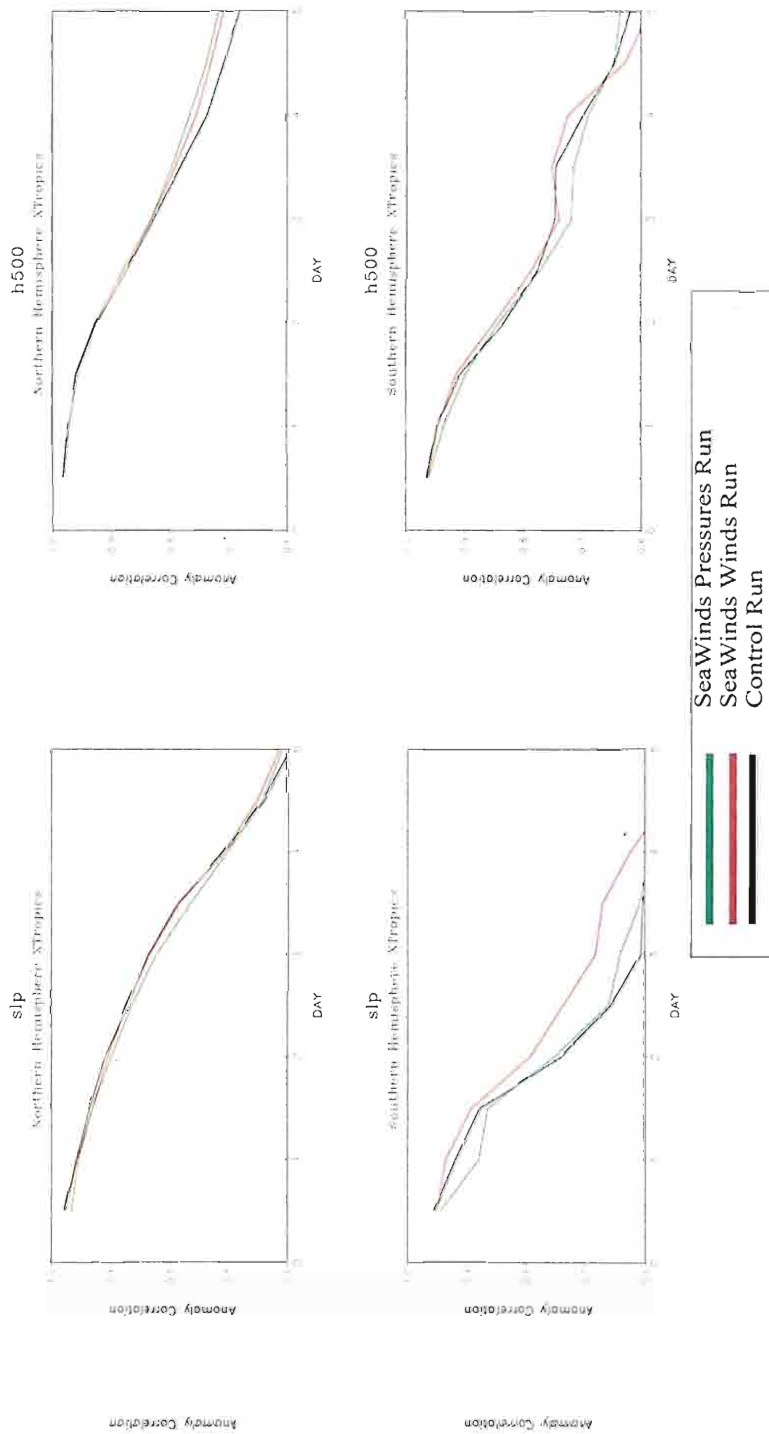
Figure 7A: Anomaly corellations of SLP and 500 hPa geopotential heights determined for forecasts made on November 9, 2000 for each of the three model runs (Control Run, Pressures Run, Winds Run)
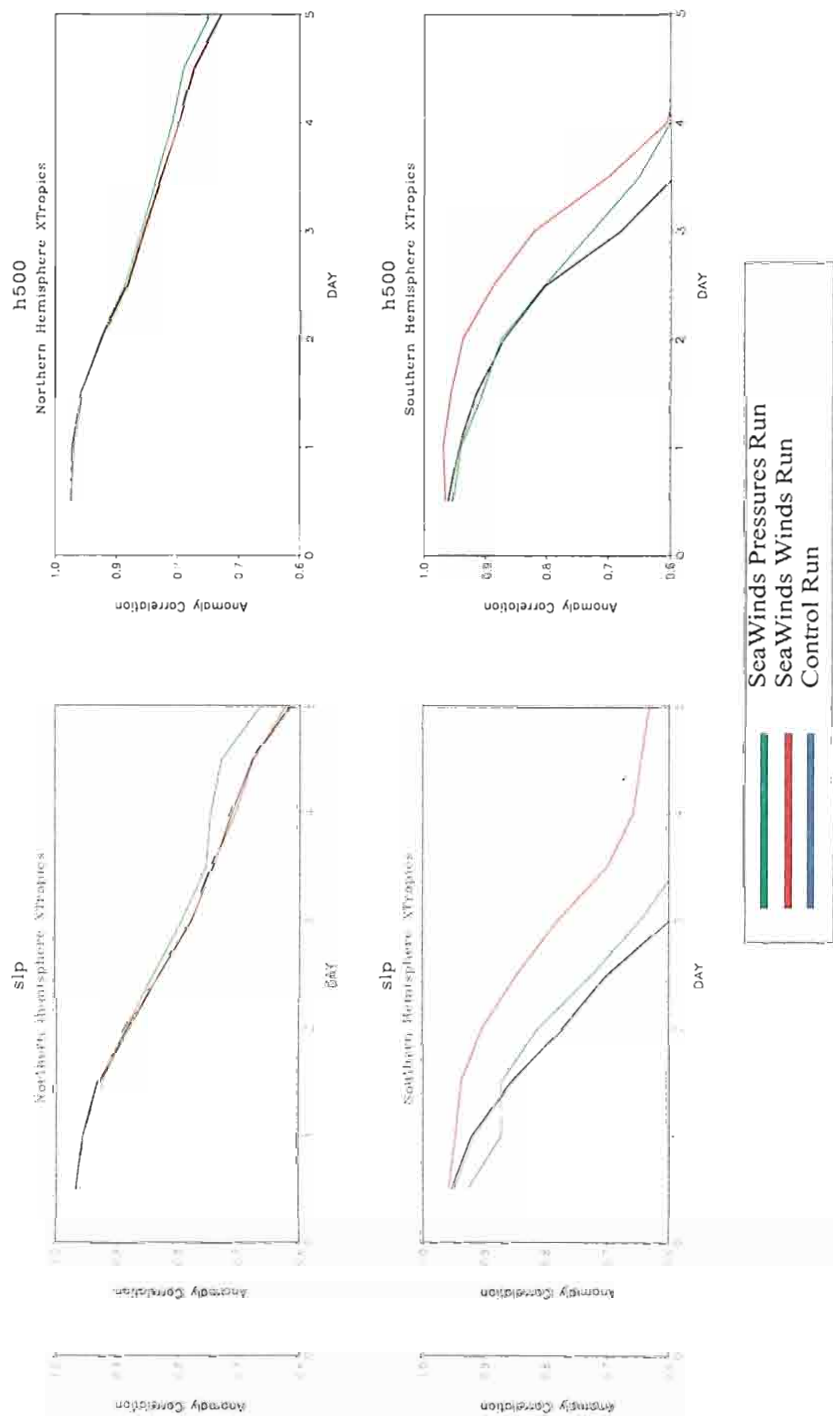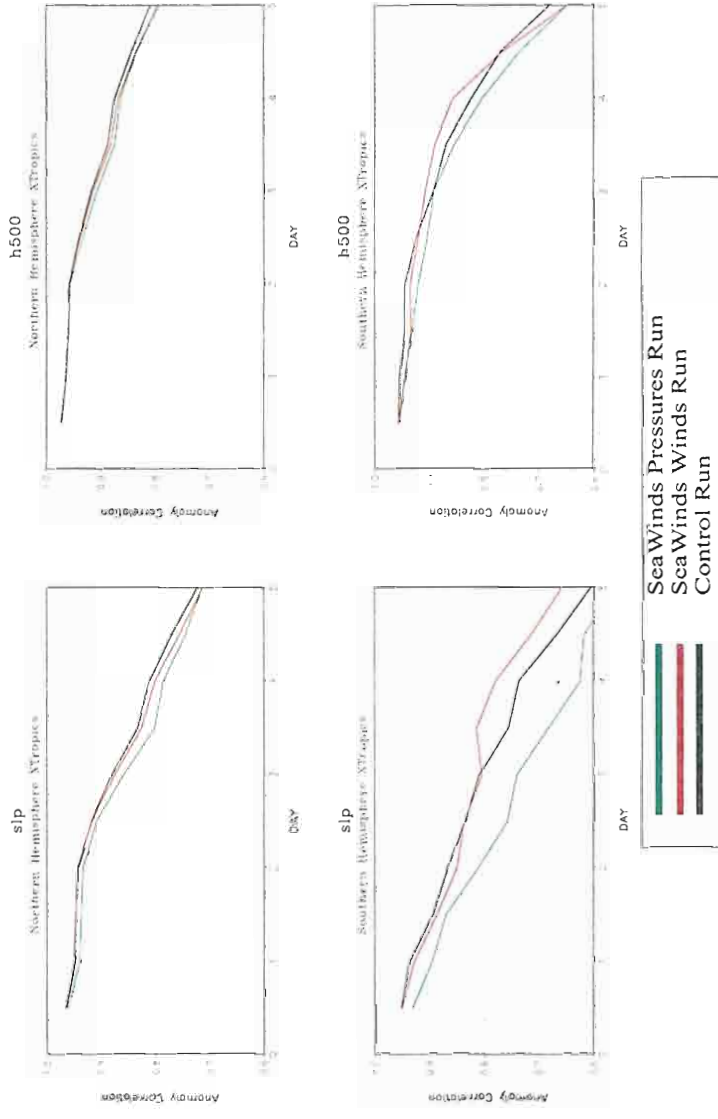
Figur Figure 7B: Anomaly corellations of SLP and 500 hPa geopotential heights determined for
forec: forecasts made on November 12, 2000 for each of the three model runs (Control Run,
Press Pressures Run, Winds Run)

Figure 7C. Anomaly corellations of SLP and 500 hPa geopotential heights determined for forecasts made on November 18, 2000 for each of the three model runs (Control Run, Pressures Run, Winds Run)

Figure 7D. Anomaly corellations of SLP and 500 hPa geopotential heights determined for forecasts made on November 22, 2000 for each of the three model runs (Control Run, Pressures Run, Winds Run)

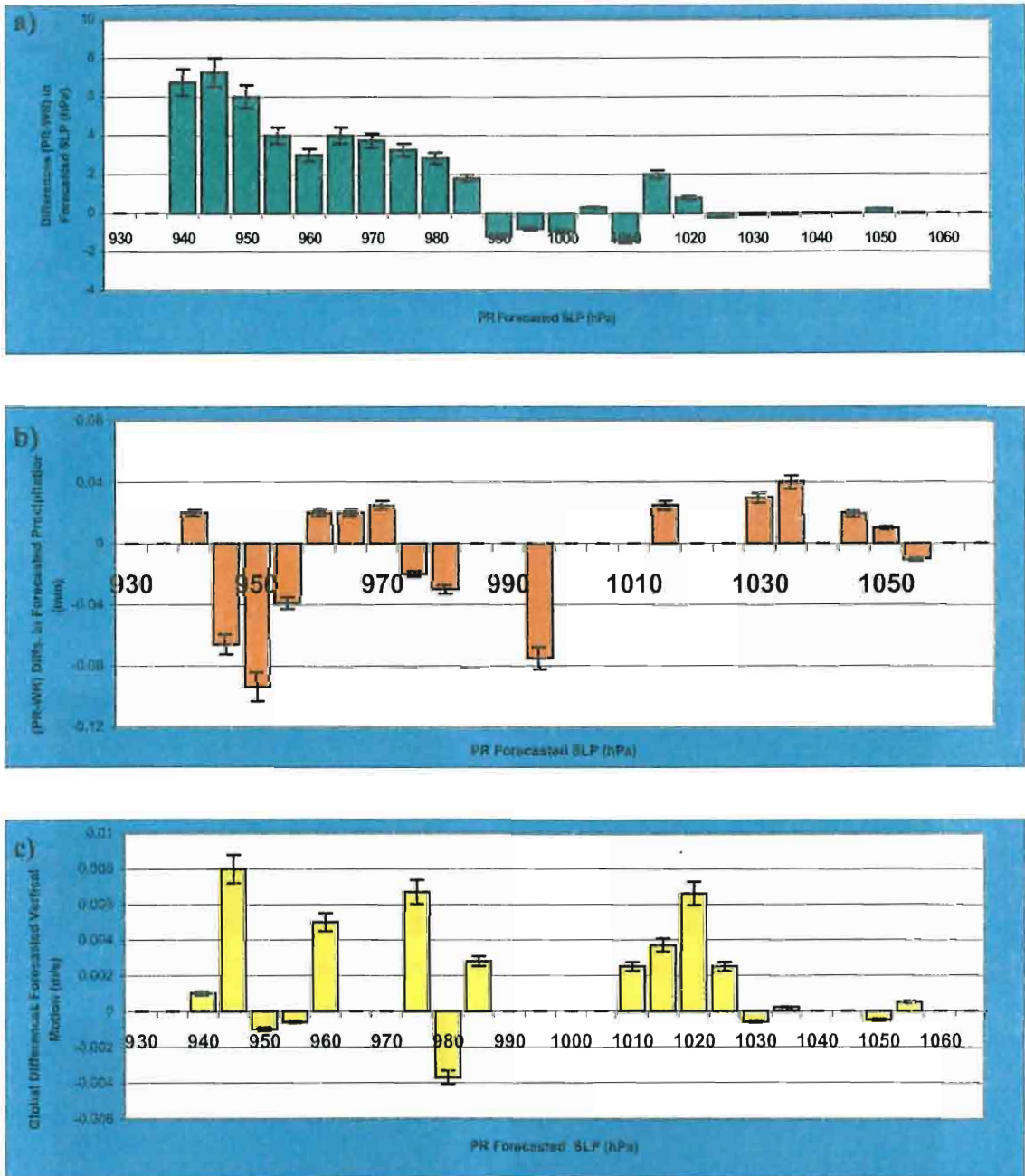**Mean Differences of SeaWinds Forecast Fields (PR – WR)**

Figure 8. Mean Differences of forecasted fields using scatterometer data (PR-WR) as a function of PR SLP. Shown are a) mean differences in SLP, b) Precipitation, and c) Vertical Velocity (omega) computed over the first 60hrs of the forecast and using the PR SLP values as the baseline. of forecasted fields using scatterometer data (PR-WR) as a function of PR SLP. Shown are a) mean differences in SLP, b) Precipitation, and c) Vertical Velocity (omega) computed over the first 60hrs of the forecast and using the PR SLP values as the baseline .

38

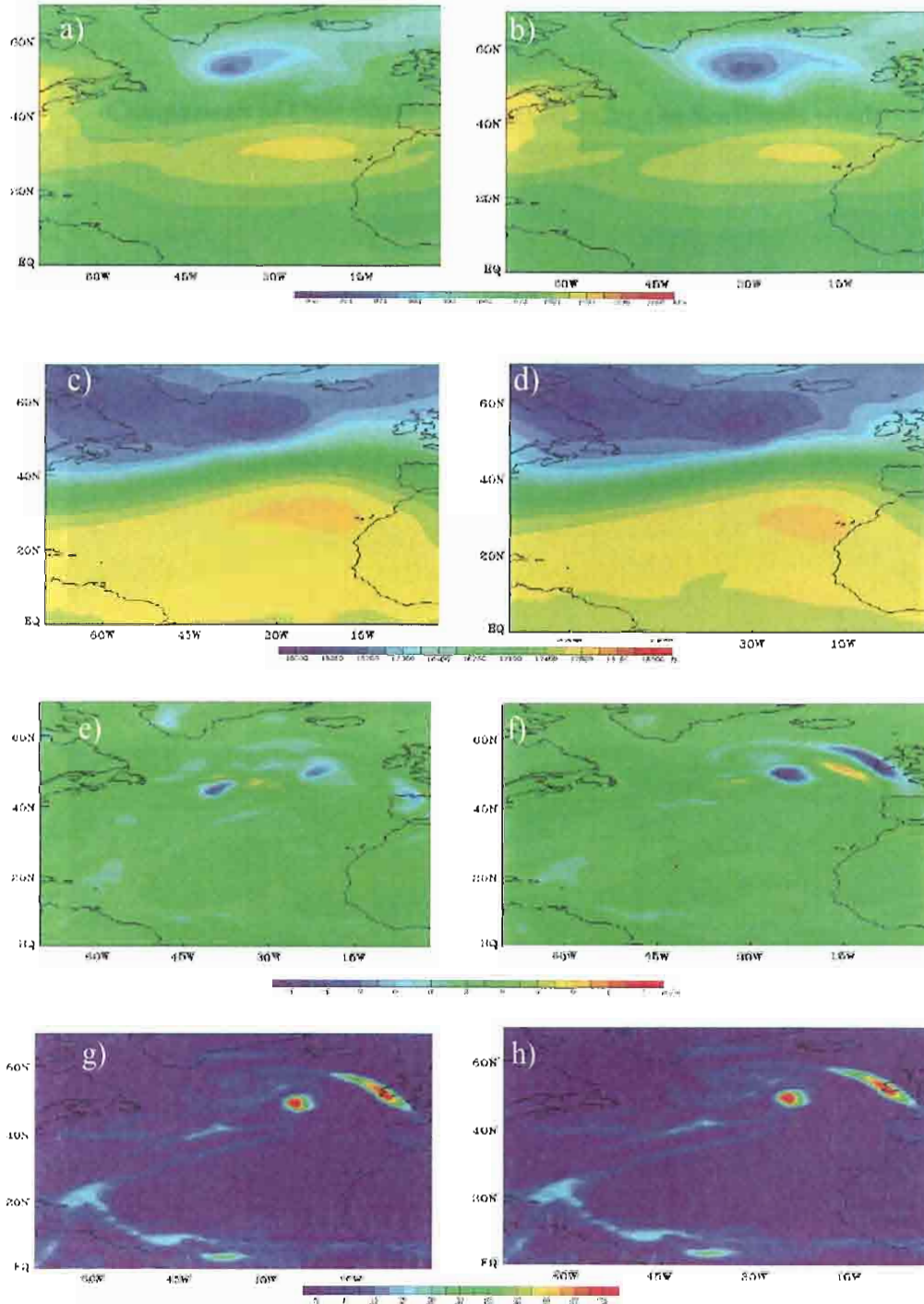# Case Study of Forecasts using the SeaWinds Pressures

Figure 9.. Forecast Results from the November 22nd forecast cycle using the SeaWinds surface pressures. Focus is drawn to is activity in the North Atlanticon November 24th.

Figure 9.. Forecast Results from the November 22nd forecast cycle using the SeaWinds surface pressures. Focus is drawn to is activity in the North Atlanticon November 24th. Shown are a) SLP, b)500hPa geopotential heights, c) vertical velocity (omega) d) total precipitation at 6Z. Corresponding values of the same parameters at 18 Zare shown in e), f), g), and h)

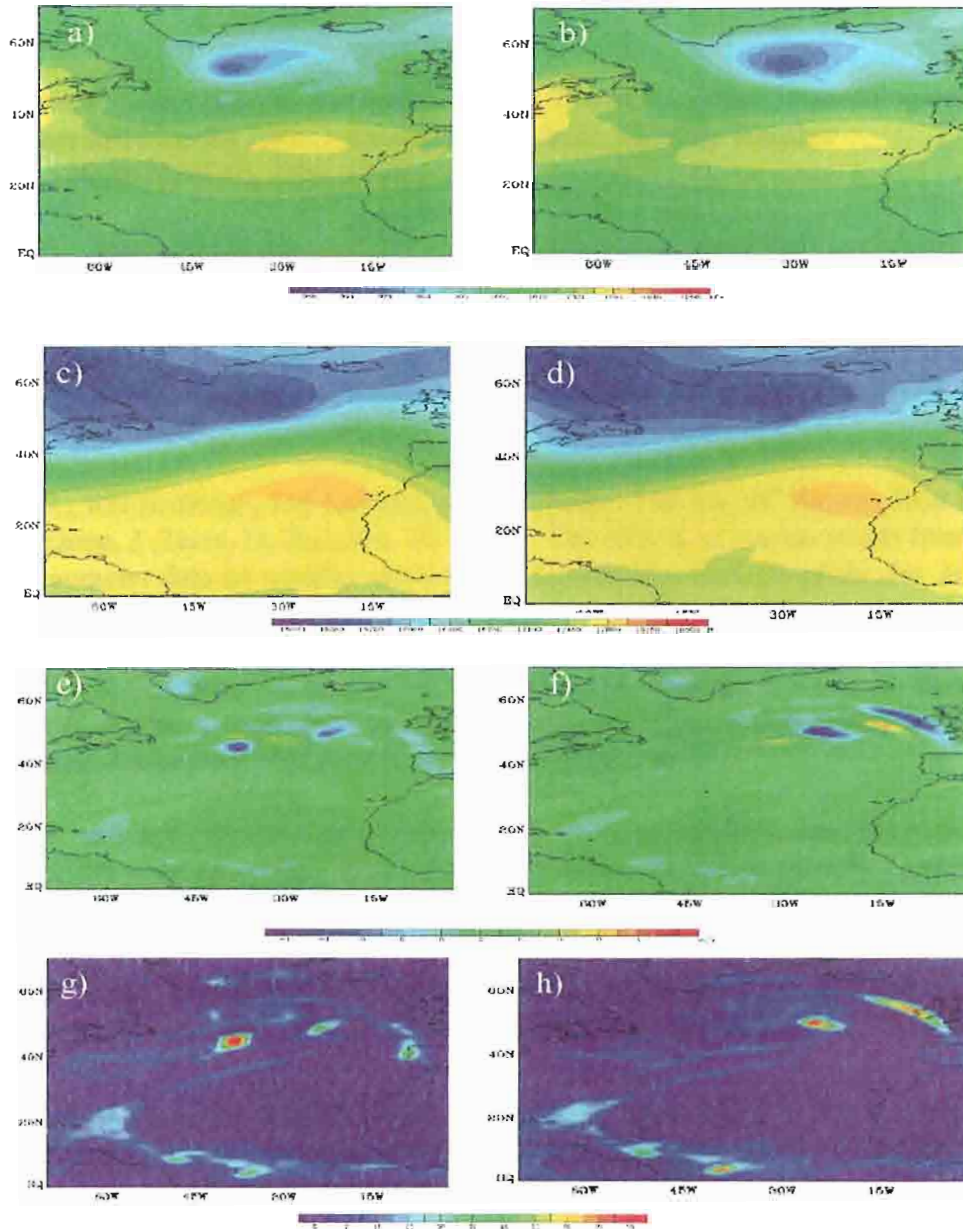# Comparison of Case Study of Forecasts using the SeaWinds winds

Figure 10. Forecast Results from the November 22nd forecast cycle using the SeaWinds surface winds Focus is drawn to is activity in the North Atlantic on November 24th. Shown are a) SLP, b)500hPa geopotential heights, c)vertical velocity (omega),d) total precipitation at 6Z. Corresponding values of the same parameters at 18 Zare shown in e), f), g), and h)

REFERENCES

Andrews, P.L. and Bell, R. S., Optimizing the United Kingdom Meteorological Office data assimilation for ERS-1 scatterometer winds, Monthly Weather Rev.,126(3):736{746, Mar. 1998.

Atlas, R., Atmospheric observations and experiments to assess their usefulness in data assimilation., *J. Meteor. Soc. Japan*, 75(1B):111-130, 1997.

Atlas R. and R.N. Hoffman, The use of satellite surface wind data to improve weather analysis and forecasting, in Satellites, *Oceanography and Society*, pp.57-79, Elsevier, New York, 2000.

Atlas, R., RN Hoffman, SM Leidner, J Sienkiewicz, TW Yu, SC Bloom, Brin E, J. Ardizzone, J .Terry, D. Bungato, JC Jusem, The effects of marine winds from scatterometer data on weather analysis and forecasting, *Bulletin of the Am. Met Soc.*82 (9): 1965-1990, 2001

Atlas, R. , S. C. Bloom, R. N. Hoffman, E. Brin, J. Ardizzone, J. Terry, D. Bungato, and J. C. Jusem. Geophysical validation of NSCAT winds using atmospheric data and analyses. *J. Geophys. Res.*, 104(C5):11405-11424, 1999.

Atlas, R. and S. C. Bloom, Global surface wind vectors resulting from the assimilation of satellite wind speed data in atmospheric general circulation models, *Oceans,* [89]260-265, 1996.

Atlas, R., P. M. Woiceshyn, S. Peteherych, and M. G. Wurtele, Analysis of satellite scatterometer data and its impact on weather forecasting. *Oceans*, **82**, 415-420, 1982.

Baker, W. E., R. Atlas, E. Kalnay, M. Halem, P. M. Woiceshyn, S. Peteherych, and D. Edelmann, Large-scale analysis and forecast experiments with wind data from the Seasat-A scatterometer, *J. Geophys. Res.*, 89(D3):4927-4936, 1984.

Brown, R. A., and L. Zeng, Estimating central pressures of oceanic midlatitude cyclones. *J. Appl. Meteor.*, **33**, 1088-1095, 1994.

Brown, R. A., and L. Zeng, Estimating central pressures of oceanic midlatitude cyclones. *J. Appl. Meteor.*, **33**, 1088-1095, 1994.

Cane, M. A., V. J. Cardone, M. Halem, and I. Halberstam, On the sensitivity of numerical weather prediction to remotely sensed marine surface wind data: A simulation

study, *J. Geophys. Res.*, 86(C9):8093-8106, 1981.

Duffy, D.G. , R. Atlas, T. Rosmond, E. Barker, and R. Rosenberg. The impact of Seasat
scatterometer data on the numerical prediction of the *Queen Elizabeth II* storm, *J.
Geophys. Res.*,   89(D5):7238-7244, 1984.

Endlich, R. M., D. E. Wolf, C. T. Carlson, J. W. Maresca, Jr, Oceanic wind
and balanced pressure-height fields derived from satellite measurements.
Mon. Wea. Rev., **10**9, 2009-2016, 1981.

Harlan, J, Jr., and J. J. O'Brien, Assimilation of scatterometer winds into
surface pressure fields using a variational method. *J. Geophys. Res.*, **9**1,
7816-7836, 1985.

Hoffman, R. N., A preliminary study of the impact of the ERS 1 C-band scatterometer
wind data on the ECMWF global data assimilation system. *J. Geophys. Res.*, 98(C6):
10233-10244, 1993.

Kiehl, J. T., J. J. Hack, G. B. Bonan, B. A. Boville, B. P. Briegleb, D. L. Williamson, and
P. J. Rasch, Description of the NCAR Community Climate Model (CCM3). *NCAR
Technical Note*, NCAR/TN-420+STR, Boulder, CO, 152pp.DAO ATBD / D1 Next
generation model – 24, 1996.

Lin, S.-J., A finite-volume integration method for computing pressure gradient
forces in general vertical coordinates. *Q. J. Roy. Met. Soc.,* 123, 1749-1762, 1997.

Lin, S.-J., and R. B. Rood, Multidimensional flux form semi-lagrangian
transport schemes. *Mon. Wea. Rev.*, 124, 2046-2070, 1996.

Lin, S.-J., and R. B. Rood, A flux-form semi-Lagrangian general circulation model
with a Lagrangian control-volume vertical coordinate. *The Rossby-100 symposium*,
Stockholm, Sweden, 1998.

Naderi, F. M., M. H. Freilich, and D. G. Long, Spaceborne radar measurement of wind
velocity over the ocean an overview of the NSCAT scatterometer system. *Proc. IEEE*,
79:850-866, 1991.

Patoux, J. and R. A. Brown, A gradient wind correction for surface pressure
fields retrieved from scatterometer winds. *J. Appl. Meteor.*, **4**2, 133-143, 2002.

Peteherych, S., P. M., Woiceshyn, W. Appleby, L. Chu, J. Spagnol, and J. E. Overland,
High resolution marine meteorological analysis utilizing Seasat data. In J. F. R. Gower,
editor, *Oceanography from Space*, pages 581-585, 1981.

High resolution marine meteorological analysis utilizing Seasat data. In J. F. R. Gower,
editor, *Oceanography from Space*, pages 581-585, 1981.

Renka, R., Interpolation of data on the surface of a sphere, *Oak Ridge Nat.
Lab. Rep. OLNR/CSD-108*, 1982.

Stoffelen A., and P. van Beukering. Implementation of improved ERS scatterometer data processing and its impact on HIRLAM short range weather forecasts. *Monthly Weather Rev*, 121:3393-3414, 1997.

Sasaki, Y., Some basic formalisms in numerical variational analysis. *Mon. Wea. Rev.*, **108**, 875-883, 1970.

Tahara, Y. and N. Nomura, The impact of satellite scatterometer data on a global NWP model, *Asian Meteorology Online Newsletter,* Vol. 2, No. 2 June 1998.

Theaupaut, J., R. N. Hoffman, and P. Courtier, Interactions of dynamics and observations in a four-dimensional variational assimilation. *Monthly Weather Rev*, 121:3393-3414,1993.

Yu T. W. and R. D. McPherson, Global data assimilation experiments with scatterometer winds from SEASAT-A. *Monthly Weather Rev*, 112:368-376, 1984.

Zeng L. and R. A. Brown, Scatterometer observations at high wind speed. J. *Appl. Meteorology*, 37(11):1412-1420, 1998.

Zierden. D. F., M. A. Bourassa, and J. J. O'Brien, Cyclone surface pressure fields and frontogenesis from NASA scatterometer (NSCAT) winds. *J. Geophys. Res.*, **105**, 23967-23981, 2000.

BIOGRAPHICAL SKETCH

Shannon Rayne Davis was born the son of Diane and Robert Davis near the banks of the Swan River in Bigfork, Montana on May 25, 1973.Growing up he spent time in Montana, as many other parts of the West, New England, and Virginia. His undergraduate years were spent at the College of William and Mary, where earned Bachelors Degrees in Physics and History with minors in Mathematics and Philosophy in 1995. His B.S. Physics thesis in the field of nuclear and particle physics was presented and published at the proceedings of the American Physical Society's annual meeting one year before.

Since his undergraduate years, Shannon has pursued graduate studies in related fields of History and Geophyiscs before coming to FSU to study Oceanography and Meteorology. He also met his incredible wife, Xujing, during this time. Together they defended their Master's theses in the summer of 2002 before moving on to pursue their Ph.D.'s in Physical Oceanography elsewhere.